Exergy-Based and Economic Evaluation of Liquefaction Processes for Cryogenics Energy Storage

Sarah Hamdy [1], Francisco Moser [2] 🆔**, Tatiana Morosuk [2],*** **and George Tsatsaronis [2],*** 🆔

[1] Energy Engineering Department, Technische Universität Berlin, 10587 Berlin, Germany; sarah.hamdy@tu-berlin.de
[2] Institute for Energy Engineering, Technische Universität Berlin, 10587 Berlin, Germany; f.moser.k@googlemail.com
* Correspondence: tetyana.morozyuk@tu-berlin.de (T.M.); georgios.tsatsaronis@tu-berlin.de (G.T.)

Abstract: Cryogenics-based energy storage (CES) is a thermo-electric bulk-energy storage technology, which stores electricity in the form of a liquefied gas at cryogenic temperatures. The charging process is an energy-intensive gas liquefaction process and the limiting factor to CES round trip efficiency (RTE). During discharge, the liquefied gas is pressurized, evaporated and then super-heated to drive a gas turbine. The cold released during evaporation can be stored and supplied to the subsequent charging process. In this research, exergy-based methods are applied to quantify the effect of cold storage on the thermodynamic performance of six liquefaction processes and to identify the most cost-efficient process. For all liquefaction processes assessed, the integration of cold storage was shown to multiply the liquid yield, reduce the specific power requirement by 50–70% and increase the exergetic efficiency by 30–100%. The Claude-based liquefaction processes reached the highest exergetic efficiencies (76–82%). The processes reached their maximum efficiency at different liquefaction pressures. The Heylandt process reaches the highest RTE (50%) and the lowest specific power requirement (1021 kJ/kg). The lowest production cost of liquid air (18.4 €/ton) and the lowest specific investment cost (<700 €/kW$_{char}$) were achieved by the Kapitza process.

Keywords: cryogenic energy storage; air liquefaction; exergy analysis; economic analysis; exergoeconomic analysis

1. Introduction

The interest in electricity storage has significantly increased with higher shares of intermittent renewable energy sources in the grid. In particular, grid-scale electricity storage with low costs are considered suitable to integrate renewable electricity generation and introduce flexibility to the power grid. Cryogenics-based energy storage (CES), frequently referred to as liquid air energy storage (LAES), is the only energy storage technology so far, which is capable to store large quantities of electricity without geographical limitations or a substantial negative environmental impact.

The thermo-electric energy storage technology stores electricity in the form of a liquefied gas (air) at a cryogenic temperature. The integrated methods of operation (charge, storage, discharge) are displayed in Figure 1. An energy-intensive liquefaction process forms the charging process of CES. The liquefied gas (cryogen) is stored in a site-independent insulated storage tank at approximately ambient pressure and a cryogenic temperature (e.g., −194 °C). The compression process of the liquefaction is presented separately, as in the adiabatic CES the heat of compression is recovered and stored to be used in the discharge process. In the discharge process, the liquefied gas is pumped to supercritical pressure in a cryogenic pump, evaporated and superheated, with thermal energy

provided by the heat storage, and supplied to a series of expanders regaining a part of the electricity charged to the system.
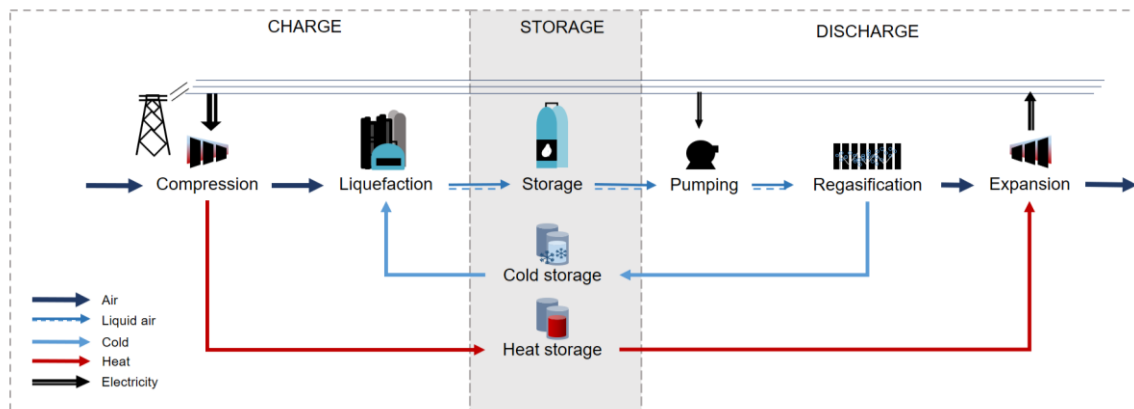

Figure 1. Illustration of cryogenic energy storage steps of operation (charge, storage, discharge), heat and cold recovery and storage.

The cold exergy rejected during the evaporation process is stored in order to increase the efficiency of the liquefaction process (charge). The CES system is composed of well-known components from the industrial gas and liquefied natural gas (LNG) supply chain.

As CES systems are based on mature technology, developers expect comparatively fast progress towards commercialization, competitive costs and efficiency enhancement. CES exergy densities are by approximately two orders of magnitudes higher than of competing technologies such as pumped hydro and compressed air energy storage reaching values higher than 430 kJ/kg. A detailed comparison of CES characteristics to other energy storages can be found in [1]. Moreover, long cycle life, low storage costs, the economy of scale and the independent sizing of charge and discharge unit speak for economic viability. Yet, the adiabatic CES systems upper limit to efficiencies is 45–50%. The thermal integration at the system level is crucial to its performance, which is the reason why the integration of cold storage into the liquefaction process is the subject of this paper.

State of the Art

Both, cryogenic energy storage and air liquefaction, are no new concepts. Large-scale air liquefaction for industrial purposes became commercial in the 1940s [2] and the first conception of storing electricity in liquid air dates back to the year 1977 [3].

Nowadays CES is rated as a pre-commercial technology being evaluated with a technology readiness level (TRL) of about 8 [4]. The CES concept was confirmed viable in testing, after Mitsubishi extended an existing air liquefier with the first pilot cryogenic power recovery unit (2.6 MW) [5]. The second pilot plant was the first integrated CES plant (350 kW/2.5 MWh) which was the result of joint research between the University of Leeds and Highview Power Storage Ltd. (London, UK) in the year 2011. The results were published in 2015: the CES economic viability was confirmed and a positive outlook on performance and costs was given [6]. A demonstration plant of 5 MW/15 MWh started operation in 2018, demonstrating a number of balancing services [7].

The significance of the liquefaction process to the CES's performance was addressed by [8] as "the key part" of the system as the discharge unit is relatively simple and efficient. The liquefaction was found to account for more than 70% of the overall exergy destruction (MW) of the CES system by the authors in a comparative exergy analysis of two 10 MW CES systems [9].

One of the key findings from the testing of the first pilot plant was the significant increase of system efficiency by cold recovery and storage [6]. The effect of cold recycle was firstly quantified by the authors as the introduction of cold storage doubled the liquid yield of the liquefaction process of the analyzed system [9].

Large-scale air liquefaction has been commercial for several decades. A number of processes exist. The simplest (no moving parts) and first-industrialized configuration is the Linde process, where purified compressed air is cooled and undergoes isenthalpic (free) expansion in a throttling valve, thus brought to its due point by the Joule-Thomson effect [10]. Gas liquefaction is nowadays performed in more complex configurations [11].

Recently, a number of publications have discussed the thermodynamic performance of CES. In the reviewed literature, CES systems with different liquefaction processes, pressures and cold storage configurations are presented in Table 1. Two kinds of a cold storage configuration are presented: (1) quartzite gravel based packed bed store with dry air as secondary working fluid, and (2) a two-tank fluid storage with methanol and propane (or R218) as secondary working fluids and storage media on two different temperature levels.

The liquid yield γ, the ratio between the mass flow of the air liquefied in the liquefaction process and the mass flow of the compressed air, is an indication of the charging-unit performance. The liquid yield varies strongly from one publication to the other. The liquid yield increases with liquefaction pressure. Yet, with increased pressures, the power consumption of the compression process increases as well. This is why the liquid yield cannot be considered as the sole indicator for the performance of the liquefaction process.

In general, different assumptions are made in the different references, e.g., ideal dry air was assumed, heat and pressure losses in most components as well as heat losses in the cold box were neglected [12], or assumed lower than 8% [6] which is why comparing the various configurations is problematic.

Three comparative evaluations of air liquefaction processes in CES systems were presented in [8,13,14]. Borri et al. [13] compared three air liquefaction processes (Linde-Hampson, Claude, Collins) for application in a micro-scale CES. The Claude process was identified as the most suitable air liquefaction process. The Linde-Hampson process (with a Joule-Thomson valve only) was found to be inferior and the second cold expander used in the Collins process was claimed to be economically not feasible. Yet, the integration of cold recovery and storage was not considered. Li [8] came to the same conclusion, that the throttle-valve-based Linde-Hampson system is not applicable for CES. Therefore, only the integration of a cold expander instead of a throttling valve in the Linde process and an expander process, employing a refrigeration process with Helium as working fluid, are compared in [8].

Table 1. Parameters of CES systems presented in [5,8,9,12,14–19]: Liquefaction processes, liquefaction pressure p_{char}, liquid yield γ, cold storage configuration, discharge pressure p_{dis} and round trip efficiency η_{RTE}.

Source	Process	p_{char}, bar	γ, -	Cold Storage Configuration	p_{dis}, bar	η_{RTE}, %
[12]	Linde-Hampson	120	0.83	fluid tanks (CH_4O, C_3H_8)	50	50–60
[15]	Integr. Linde-Hampson	90	0.60	fluid tanks (CH_4O, C_3H_8)	120	60
[9]	Heylandt	180	0.61	fluid tanks (CH_4O, R218)	150	41
[16]	Modified Claude	180	0.86	packed bed gravel (air)	75	48.5
[17]	2 Turbine Claude/Collins	54	NA	packed bed gravel (air)	150	47
[6]	4 Turbine Claude	56.8	0.551 [1]	packed bed gravel (air)	190	>50
[18]	Linde-Hampson	180	0.842	fluid tanks (CH_4O, C_3H_8)	65	50
[19]	Linde-Hampson	140	NA	NA	70	47.2
[11]	Linde-Hampson	20	0.70	direct integration (ideal)	100	20–50
[8]	Linde-Hampson [2]	~130	0.44–0.74	fluid tanks (CH_4O, R218)	112–120	28–37
[8]	Expander cycle	NA	NA	fluid tanks (CH_4O, R218)	NA	40–46
[20]	Single expander	135	0.84	fluid tanks (CH_4O, C_3H_8)	80	50–58

[1] calculated from: 12 h charging, 3:1 (charge-to-discharge ratio), $\dot{m}_{char}$ = 34.1 kg/s. [2] with cold expander/throttling valve.

Abdo et al. [14] compared the by Chen et al [21] patented CES system design based on a simple Linde-Hamson liquefaction process to two alternative systems based on the Claude and the Collins process. The heat of compression was taken into account but cold storage was not comprised.

The Claude and Collins process showed similar thermodynamic performance with greater RTE that the Linde based system. Despite the Linde-Hampson having the lowest specific costs, the Claude-based system was evaluated the best option. The present paper aims to compare a number of air liquefaction process configurations with integrated cold storage in order to identify the most suitable process for implementation in CES systems.

2. Methods

For a comparative analysis, six liquefaction processes were simulated with and without integration of cold storage under similar conditions. Results from energetic, exergetic, economic and exergoeconomic analyses were used to identify the most cost-effective liquefaction process for CES with cold storage.

2.1. Design and Simulation

Aspen Plus® (Version 9, Aspen Technology Inc., Bedford, MA, USA) was chosen as a suitable software for process simulation. With the aid of the simulation software, all mass and energy balances are fulfilled and the specific enthalpy and entropy values of all streams and substances are calculated. The Peng-Robinson equation of state was employed and the simulation was performed under steady-state conditions. Fortran routines are integrated to calculate exergy values for the exergetic analysis. Six liquefaction processes were simulated: the simple Linde, the precooled Linde, the dual pressure Linde, the simple Claude, the Kapitza and the Heylandt process. At first, the liquefaction processes were manually optimized and later modified to accommodate the cold storage. The assumptions made in simulation are given in Table 2.

Table 2. Assumptions made in simulation.

Parameter	Value, Unit
Isentropic efficiencies (compressors, expanders)	$\eta_{is,CM}$ = 87% [8], $\eta_{is,EX}$ = 80% [17]
Intercooler exit temperature and pinch	$T_{exit, IC}$ = 25 °C, $\Delta T_{pinch, IC}$ = 5 K [15]
Main heat exchanger pinch temperature difference	$\Delta T_{pinch, MHE}$ = 1–3 K [8,17]
Maximal pressure of compression	$p_{max, CM}$ = 200 bar [22]
Ambient conditions	T_{amb} = 15 °C, p_{amb} = 1.013 bar

The overall system configuration is shown in Figure 2. The pretreated air enters the analyzed system at 15 °C, 1.013 bar and a molar composition of 79% N_2 and 21% O_2 (a1). The compression block is the same for all systems. The air exits the last intercooler of the three-stage compression at a temperature of 25 °C and a pressure of $p_{max,CM}$ of 200 bar (a2). The largest part of the thermal energy increase during compression is recovered in a heat storage. The heat storage is realized with pressurized water tanks (5 bar, 205 °C). The design of the liquefaction block is different for each system. Two types of liquefaction processes can be distinguished: Linde-based (Figure 3) and Claude-based (Figure 4) liquefaction processes. The liquefied air exits the flasher and is stored at a temperature of −192 °C and slightly elevated pressure 1.3 bar. The liquid is stored in an insulated storage tank with boil-off losses of 0.2 %$_{Vol}$.
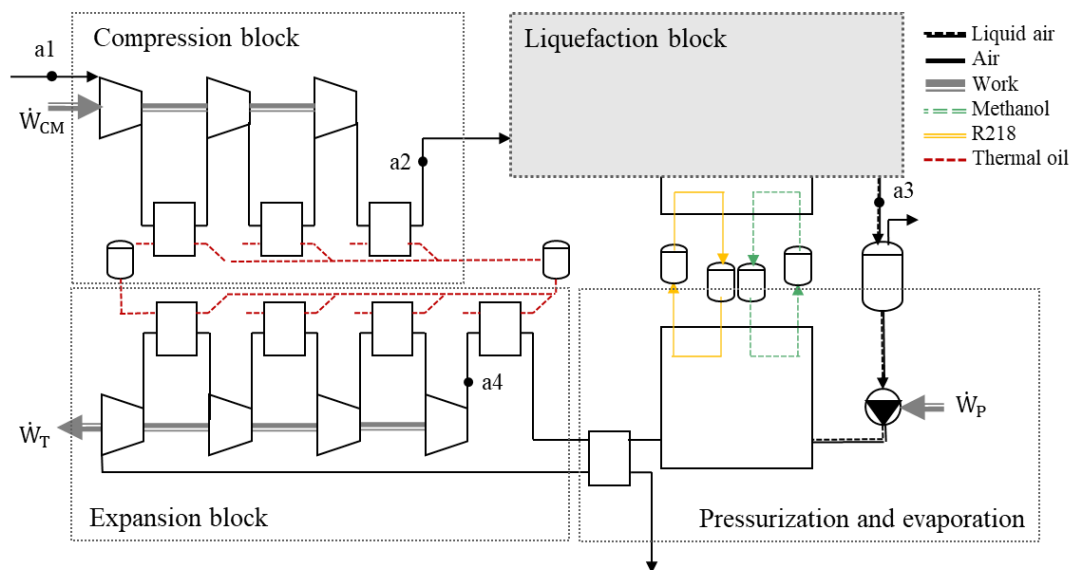
Figure 2. Flowsheet of the adiabatic CES system with "black box" air liquefaction block.
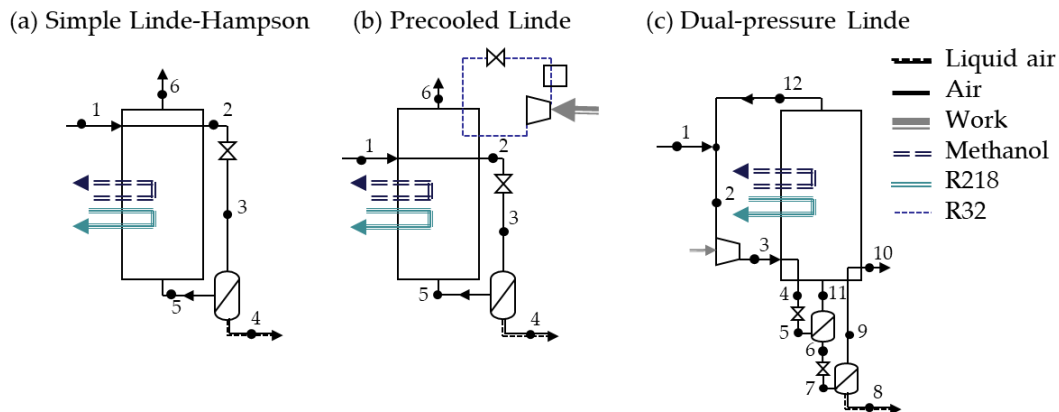

Figure 3. Flowsheets of Linde-based air liquefaction processes with cold recycle.
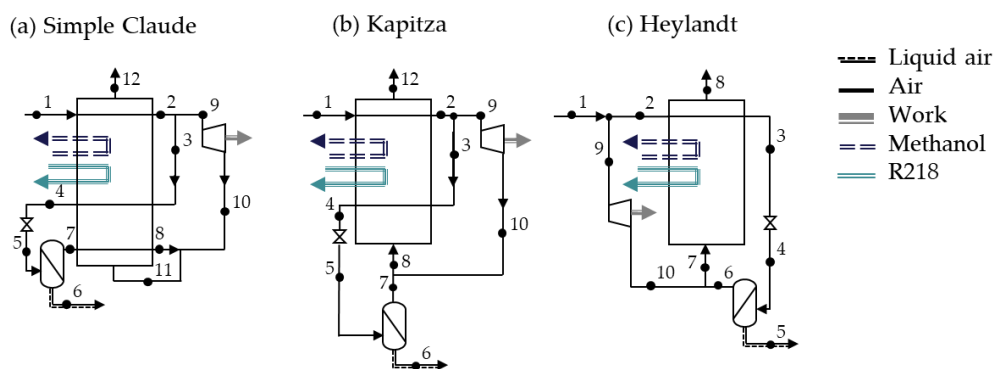

Figure 4. Flowsheets of Claude-based air liquefaction processes with cold recycle.

During discharge, the liquid air is pressurized to 150 bar, evaporated in heat exchange to the cold storage media, superheated (T_{a4} = 195 °C) and fed to the four-stage expander with reheat. The specific power output of the discharge unit is constant for all systems (w_{dis} = 470 kJ/kg of liquid air).

The assumed method of cold storage uses two fluid tanks and two circulating working fluids that recover the high-grade and low-grade cold rejected in the evaporation process. Reviewing a number of refrigerants, *R218* and *methanol* are shown to be advantageous with respect to toxicity, flammability, boiling and freezing temperatures [9]. The cold in the temperature interval −180 to

−61 °C is recovered by *R218*, while the cold at higher temperatures (−19 to −59 °C) is captured and stored using *methanol*. The amount of cold recovered is determined by the amount of air liquefied in the liquefaction process. The mass flow rates of the cold storage media are therefore determined by a ratio of the mass flow rate of the liquefied air $\dot{m}_{a3}$:

$$\dot{m}_{R218} = 2.29 \cdot \dot{m}_{a3} \tag{1}$$

$$\dot{m}_{methanol} = 0.49 \cdot \dot{m}_{a3} \tag{2}$$

The ratio is adjusted to the optimal heat transfer between the evaporating liquid air and the cold storage media. Thermal losses in the cold storage were accounted for and are equivalent to 4 K/cycle.

The liquefaction processes are shown in Figures 3 and 4. A detailed description of the liquefaction processes and the fundamental concept can be found in fundamental publications e.g., [23]. The stream values (mass flow $\dot{m}$, temperature T and pressure p) can be found in Tables 3 and 4.

The Linde-Hampson process, Figure 3a, is the most straightforward of all liquefaction processes. The process consists of only four sets of components: the compressor(s), the main heat exchanger (MHE), the throttling valve and the flash tank. After compression, the temperature of the air is reduced (below −100 °C) in the MHE. The low-temperature high-pressure air is throttled reducing the temperature close to the dew point resulting in partial condensation. In the flash tank, the liquid air is separated and stored. The gaseous air is supplied back to the MHE to precool the compressed air. The efficiency of the simple Linde-Hampson process strongly depends on the temperature of the high-pressure gas at the inlet of the MHE.

The precooled Linde-Hampson process, shown in Figure 3b, intends to achieve a better performance and a higher liquid yield by lowering the temperature of the air with the addition of a compression refrigeration process. Working fluids such as ammonia, carbon dioxide or Freon compounds are commonly used for the secondary refrigeration cycle.

In the dual-pressure Linde process (Figure 3c) the heat transfer in the MHE is improved by introducing a second pressure level. The air enters the liquefaction process at an intermediate-pressure (1). Together with the recycled stream, the pressure of the air is elevated further to the high-pressure level (3). The gas is cooled and throttled to the intermediate-pressure level (5). The gaseous and the liquid air are separated in the intermediate-pressure flash tank. The gaseous part is fed back to the MHE to precool the entering air stream (3) to (4) and is mixed to the entering intermediate-pressure air stream (1). The liquefied air is fed to the second pressure-stage. This modification reduces the specific work required to liquefy the air at the expense of the share of air liquefied.

The Claude process and its modifications are the most commonly employed process in commercial air liquefaction plants, as its efficiency is higher than that of the Linde process [23]. In the Claude process the cooling of compressed air is provided by a cold recycle stream—a part of the pressurized air that underwent an isentropic expansion in cold expanders [6]. The application of a cold expander avoids part of the exergy destruction in the throttling process and reduces the required power for liquefaction by the power output of the expander ($\dot{W}_{char} = \sum \dot{W}_{CM} - \dot{W}_{EX}$). The stream exiting the expander ($\dot{m}_{10}$) is used to cool the air stream entering the MHE. The expander does not replace the throttling valve before the flash tank.

The Kapitza process is analogous to the Claude process but with the difference that the third partition of the MHE (or low-temperature heat exchanger) is eliminated. In other words, while using a multi-stream heat exchanger, stream 7 is not fed to the MHE before mixing. Streams 7 and 10 tend to have only a small temperature difference, which is why the difference in heat exchanger area and performance is little. The Heyland process is also adopted from the Claude process. Nevertheless, it can also be seen as a variation of the precooled Linde-Hampson process using air as a refrigerant. The precooling process—the splitting of the stream before entering the MHE—improves the heat transfer process in the MHE [23].

Table 3. Stream values for the states indicated in the flowsheets in Figure 3.

Stream	Variable, Unit		Simple Linde With Storage		Precooled Linde With Storage		Dual-Pressure Linde With Storage	
1	$\dot{m}$	kg/h	100.0	100.0	100.0	100.0	100.0	100.0
	T	°C	25.0	25.0	25.0	25.0	25.0	25.0
	p	bar	200.0	200.0	200.0	200.0	33.4	33.4
2	$\dot{m}$	kg/h	100.0	100.0	100.0	100.0	547.3	137.3
	T	°C	−102.4	−125.3	−113.6	−138.7	24.1	24.2
	p	bar	200.0	1.03	200.0	200.0	30.4	30.4
3	$\dot{m}$	kg/h	100.0	100	100	100	547.3	137.3
	T	°C	−191.8	−191.7	−192.3	−193.1	25.0	25.0
	p	bar	1.03	1.03	1.03	1.03	200.0	200.0
4	$\dot{m}$	kg/h	9.0	31.2	19.8	44.1	547.3	137.3
	T	°C	−191.8	−192.7	−192.3	−193.1	−105.0	−124.5
	p	bar	1.03	1.03	1.03	1.03	200.0	200.0
5	$\dot{m}$	kg/h	91.0	68.8	80.2	55.9	547.3	137.3
	T	°C	−191.8	−192.7	−192.3	−193.1	−146.2	−146.2
	p	bar	1.03	1.03	1.03	1.03	30.4	30.4
6	$\dot{m}$	kg/h	91.0	68.8	80.2	55.9	100.0	100.0
	T	°C	24.0	24.0	24.0	−95.8	−146.2	−146.2
	p	bar	1.03	1.03	1.03	1.03	30.4	30.4
7	$\dot{m}$	kg/h	-	-	-	-	100.0	100.0
	T	°C	-	-	-	-	−192.9	−192.9
	p	bar	-	-	-	-	1.03	1.03
8	$\dot{m}$	kg/h	-	-	-	-	40.0	40.0
	T	°C	-	-	-	-	−193.0	−193.0
	p	bar	-	-	-	-	1.03	1.03
9	$\dot{m}$	kg/h	-	-	-	-	60.0	60.0
	T	°C	-	-	-	-	−193.0	−193.0
	p	bar	-	-	-	-	1.03	1.03
10	$\dot{m}$	kg/h	-	-	-	-	60.0	60.0
	T	°C	-	-	-	-	24.0	24.0
	p	bar	-	-	-	-	1.03	1.03
11	$\dot{m}$	kg/h	-	-	-	-	447.3	37.3
	T	°C	-	-	-	-	−146.2	−146.2
	p	bar	-	-	-	-	30.4	30.4
12	$\dot{m}$	kg/h	-	-	-	-	447.3	37.3
	T	°C	-	-	-	-	24.0	24.0
	p	bar	-	-	-	-	30.4	30.4

Table 4. Stream values for the states indicated in the flowsheets in Figure 4.

Stream	Variable, Unit		Claude With Storage		Kapitza With Storage		Heylandt With Storage	
1	$\dot{m}$	kg/h	100.0	100.0	100.0	100.0	100.0	100.0
	T	°C	25.0	25.0	25.0	25.0	25.0	25.0
	p	bar	200.0	200.0	200.0	200.0	200.0	200.0
2	$\dot{m}$	kg/h	100.0	100.0	100.0	100.0	36.0	76.1
	T	°C	−4.0	−2.0	−4.0	−2.0	25.0	25.0
	p	bar	200.0	200.0	200.0	200.0	200.0	200.0
3	$\dot{m}$	kg/h	34.3	73.2	34.3	73.3	36.0	76.1
	T	°C	−4.0	−2.0	−4.0	−2.0	−177.6	−180.5
	p	bar	200.0	200.0	200.0	200.0	200.0	200.0
4	$\dot{m}$	kg/h	34.3	73.2	34.3	73.3	36.0	76.1
	T	°C	−190.8	−182.8	−190.6	−182.8	−193.9	−194.0
	p	bar	200.0	200.0	200.0	200.0	1.03	1.03
5	$\dot{m}$	kg/h	34.3	73.2	34.3	73.3	28.6	62.3
	T	°C	−194.1	−194.0	−194.1	−194.0	−193.9	−194.0
	p	bar	1.03	200.0	1.03	1.03	1.03	1.03
6	$\dot{m}$	kg/h	31.2	61.5	31.1	61.5	7.4	13.7
	T	°C	−194.1	−194.0	−194.1	−194.0	−176.5	−179.0
	p	bar	1.03	1.03	1.03	1.03	1.03	1.03
7	$\dot{m}$	kg/h	3.1	11.8	3.2	11.8	71.4	37.7
	T	°C	−194.1	−194.0	−194.1	−194.0	−176.4	−177.4
	p	bar	1.03	1.03	1.03	1.03	1.03	1.03
8	$\dot{m}$	kg/h	3.1	11.8	68.9	38.5	71.4	37.7
	T	°C	−192.0	−191.0	−191.7	−192.1	−7.3	24.0
	p	bar	1.03	1.03	1.03	1.03	1.03	1.03
9	$\dot{m}$	kg/h	65.7	26.8	65.7	26.7	64.0	24.0
	T	°C	−4.0	−2.0	−4.0	−2.0	25.0	25.0
	p	bar	200.0	200.0	200.0	200.0	200.0	200.0
10	$\dot{m}$	kg/h	65.7	26.8	65.7	26.7	64.0	24.0
	T	°C	−191.6	−191.2	−191.6	−191.2	−176.4	−176.4
	p	bar	1.03	1.03	1.03	1.03	1.03	1.03
11	$\dot{m}$	kg/h	68.8	73.0	-	-	-	-
	T	°C	−191.7	−182.8	-	-	-	-
	p	bar	1.03	200.0	-	-	-	-
12	$\dot{m}$	kg/h	68.8	38.6	68.9	73.3	-	-
	T	°C	24.0	23.4	24.0	24.0	-	-
	p	bar	1.03	1.03	1.03	1.03	-	-

The performance of the Claude-based processes is dependent on the splitting ratio r. The splitting ratio is defined as the mass flow through the expander $\dot{m}_{EX}$ over the mass flow through the last compression step $\dot{m}_{CM}$:

$$r = \frac{\dot{m}_{EX}}{\dot{m}_{CM}} \tag{3}$$

The Kapitza process dates back to 1939 when the inventor suggested the use of centrifugal expansion turbines in the Claude process [10]. Most modern liquefiers utilize expansion turbines proposed by Kapitza [10,24] and most high-pressure air liquefaction plants operate with the Heylandt process. Highview Power Storage Ltd. base their charging unit on the Claude process relying on the maturity of the process and the trouble-free scale-up [25]. The pilot plant operates with a Claude-based liquefaction process similar to the Kapitza configuration [26]. The operation pressures for the different

liquefaction processes differ [23]. For a better comparison, the liquefaction pressure is kept to 200 bar [23] first and later varied in sensitivity analysis.

2.2. Energetic and Exergetic Analyses

The six liquefaction processes were compared with and without cold storage in energetic and exergetic analyses at the system level. For the three most efficient processes, sensitivity analyses and exergetic analyses at the component level were further undertaken. The exergetic analysis is adopted from [27]. The exergetic efficiency ε, the liquid yield γ and the specific power requirement w of the systems were used as a basis for comparing the process' performance with and without cold recovery. The parameters are defined below:

$$\varepsilon = \frac{\dot{E}_{liquid\ air} + \dot{E}_{q,hot}}{\dot{W}_{char} + \dot{E}_{q,cold}} [-] \tag{4}$$

$$\gamma = \frac{\dot{m}_{liquid\ air}}{\dot{m}_{CM}} [-] \tag{5}$$

$$w = \frac{\dot{W}_{char}}{\dot{m}_{liquid\ air}} \left[\text{kJ/kg}_{\text{liquid air}}\right] \tag{6}$$

The general definition of the exergetic efficiency ε is the ratio of the exergy of the product $\dot{E}_P$ and the exergy of the fuel $\dot{E}_F$. The fuel supplied to the liquefaction system is the charging power $\dot{W}_{char}$ and the exergy of the low-temperature exergy supplied by the cold storage $\dot{E}_{q,cold}$:

$$\dot{W}_{char} = \sum \dot{W}_{CM} - \dot{W}_{EX} \tag{7}$$

$$\dot{E}_{q,cold} = \left| (1 - T_0/T_{cold}) \cdot \dot{Q}_{cold} \right| = \dot{m}_{liquid} \cdot \Delta e_{R218} + \dot{m}_{methanol} \cdot \Delta e_{methanol} \tag{8}$$

T_{cold} (or T_{hot}) denote the thermodynamic mean temperatures at which the low-temperature energy (or the heat) is supplied. Both the exergy of the liquefied air $\dot{E}_{liquid\ air}$ and the exergy of the heat supplied to the heat storage $\dot{E}_{q,hot}$ are products of the liquefaction process:

$$\dot{E}_{liquid\ air} = \dot{m}_{liquid} \cdot e_{liquid\ air} \tag{9}$$

$$\dot{E}_{Q,hot} = (1 - T_0/T_{hot}) \cdot \dot{Q}_{heat} \tag{10}$$

The definitions of fuel and product for CES system components can be found in [9]. As the systems partially operate below the ambient temperature, the physical exergy is split into its mechanical and thermal parts, according to [28].

The liquefaction processes with the best performance with cold storage were identified (200 bar) and a sensitivity analysis was performed. In sensitivity analyses the splitting ratio r and liquefaction pressure $p_{max,CM}$ were varied. For the optimal liquefaction pressure and splitting ratio, the three systems were compared using economic and exergoeconomic analyses.

The round-trip efficiency (RTE) of the systems was calculated as base for comparison. The RTE is defined as the ratio between the electricity charged and the electricity discharged:

$$\eta_{RTE} = \frac{\dot{W}_{dis}}{\dot{W}_{char} \cdot \frac{\tau_{char}}{\tau_{dis}}} \tag{11}$$

In contrast to evaluating the charging system only, for the overall system the charging duration τ_{char} and the discharge duration τ_{dis} need to be accounted for. Reason for this is that the

charge-to-discharge ratio ($\frac{\tau_{char}}{\tau_{dis}}$) may be unequal to one. For calculation of the RTE an exergy density of approx. 445–465 kJ/kg and a charge-to-discharge ratio of two was accounted for.

2.3. Economic Analysis

The economic analysis was performed on the optimal system configuration ($p_{max,CM}, r \rightarrow \varepsilon_{max}$) of the best performing processes. The processes were sized to 20 MW charging power $\dot{W}_{char}$. The total revenue requirement (TRR) method was applied [22]. The bare module costs (BMC) of the components were estimated with a number of methods. Cost estimating charts [29,30], cost estimating equations [8] and past purchase orders [27,31,32] were considered. Pressure and temperate ranges were also taken into account. The costs were adjusted to €2017 with the chemical engineering cost indexes of the reference years (CEPCI$_{2017}$ = 567.5 [33]). The derived cost equations of the BMC for each type of component can be found in [34].

The assumptions made in the economic analyses are summarized in Table 5. The operation and maintenance costs (OMC) are assumed as a percentage of the fixed capital investment (FCI) which ranges from 1.5% to 3% of the plant purchase price per year [35]. The system is assumed to operate at low electricity prices.

Table 5. Assumptions made in economic analysis.

Assumption	Value
Service facilities, architectural work	30% of BMC
Contingencies	15% of BMC
Effective interest rate	8%
Average inflation rate	3%
Plant economic life	30 years
Annual full load operation	2882 h/a
Annual OMC	1.5% of FCI
Mean cost of charged electricity	17.2 €/MWh

For better comparability the specific investment costs are determined. The total capital investment (TCI) of the charging unit is levelized to the charging capacity of the storage (€/kW$_{char}$).

For the exergoeconomic analysis, the levelized cost rate $\dot{Z}_k$ of each component k needs to be determined. The component cost rate considers the costs associated with the capital investment $\dot{Z}_k^{CI}$ and the operation and maintenance costs $\dot{Z}_k^{OM}$ of the respective component. The component cost rate is calculated over the levelized carrying charges CC_L, the levelized operation and maintenance costs OMC_L, the annual operation time of the component τ and the share of the investment costs BMC_k associated with the k-th component in the total bare-module costs BMC_{tot} of the overall system:

$$\dot{Z}_k = \dot{Z}_k^{CI} + \dot{Z}_k^{OM} = \frac{BMC_k}{BMC_{tot}} \cdot \frac{(CC_L + OMC_L)}{\tau} \tag{12}$$

2.4. Exergoeconomic Analysis

The exergoeconomic analysis was applied to the best performing liquefaction processes. Aim is to identify the cost-effectiveness of the processes, the costs associated with the thermodynamic inefficiencies and the potential for cost reduction in the processes. This is achieved by "exergy costing" [27], where the average cost per unit of exergy of each stream in the process is calculated with the aid of cost balances and auxiliary equations. The cost balance for the k-th component of the process is expressed by:

$$\sum \dot{C}_{out,k} + \dot{C}_{k,W} = \dot{C}_{k,Q} + \sum \dot{C}_{in,k} + \dot{Z}_k \tag{13}$$

The cost balance needs to be fulfilled for each component in the system to determine the costs of the exiting streams. The sum of the costs associated with the n entering streams of matter $\sum \dot{C}_{in,k}$, the

cost rate of the respective component $\dot{Z}_k$ and the cost of heat supplied to the component $\dot{C}_{k,Q}$ are equal to the sum of costs associated with the m exiting streams of matter $\sum \dot{C}_{out,k}$ and the work done by the system. Each stream of matter, heat or work with associated exergy transfer rate has an average cost per unit of exergy c_n (€/GJ):

$$\dot{C}_n = c_n \cdot \dot{E}_n \tag{14}$$

$$\dot{C}_W = c_W \cdot \dot{W} \tag{15}$$

$$\dot{C}_Q = c_Q \cdot \dot{E}_Q \tag{16}$$

All costs associated with the streams entering the overall system need to be known. The specific cost of the incoming air is set to $c_1 = 0$ €/MWh while the specific costs of the electricity is $c_W = 17.5$ €/MWh. The specific exergy costs of the entering cold storage media streams are assumed equal to the cost per unit of exergy of the liquid air:

$$c_{R218, in} = c_{methanol,in} = c_{liquid\ air} \tag{17}$$

If more than one stream exits the component, auxiliary equations based on the "fuel and product" approach are necessary [24]. The cost balance at the component level can also be formulated as:

$$\dot{C}_{P,k} = \dot{C}_{F,k} + \dot{Z}_k \tag{18}$$

The cost associated with the thermodynamic inefficiencies—the exergy destruction—is calculated by the average cost per unit of exergy of the fuel to the component $c_{F,k}$ and the exergy destruction $\dot{E}_{D,k}$ of the respective component:

$$\dot{C}_{D,k} = c_{F,k} \cdot \dot{E}_{D,k} \tag{19}$$

The components which are of high importance to the system's cost-effectiveness are determined by the sum of cost associated with the initial investment of the component $\dot{Z}_k$ and the cost associated with the exergy destruction $\dot{C}_{D,k}$. The exergoeconomic factor can be used to determine the type of changes required to improve the cost effectiveness of the respective component:

$$f = \frac{\dot{Z}_k}{\dot{Z}_k + \dot{C}_{D,k}} \tag{20}$$

In the performed exergoeconomic analysis the major contributors to the overall costs are identified and their potential for cost reduction is compared. Moreover, the results facilitate a subsequent iterative optimization.

3. Results and Discussions

3.1. Energetic and Exergetic Analyses

The results of the energetic and exergetic analysis of each liquefaction configuration before and after the integration of cold storage are shown in Figure 5. The integration of cold storage significantly increases the liquid yield. The exergy of the product increases correspondingly:

$$\dot{E}_P \uparrow = \dot{E}_{liquid\ air} \uparrow + \dot{E}_{Q,hot}. \tag{21}$$
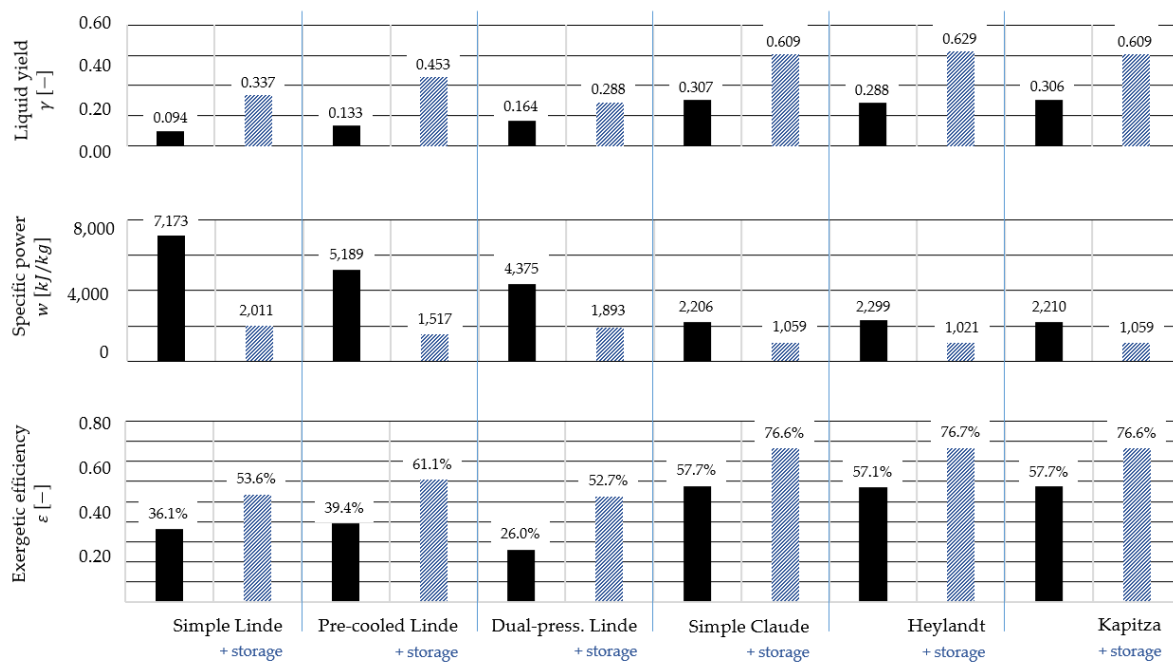
Figure 5. Results of exergy analysis of the liquefaction processes with/without integrated cold storage.

With a higher share of air liquefied the cold supplied by the cold storage increases ($\dot{E}_{cold}$ ↑). A substantial reduction of the specific power required to produce one kg of liquid air is observed for all processes ($\dot{W}_{char}$ ↓). Thus, the exergetic efficiency is considerably augmented with the addition of cold storage:

$$\varepsilon \uparrow = \frac{\dot{E}_{liquid\ air} \uparrow + \dot{E}_{Q,hot}}{\dot{E}_{cold} \uparrow + \dot{W}_{char} \downarrow} \tag{22}$$

The improvements were most significant in the simple Linde and the precooled Linde configuration where the exergetic efficiency increased significantly. Despite the liquid yield of the precooled Linde reaching a compatible value (0.453), its specific power requirement and exergetic efficiency cannot level with the Claude-based configurations. The simple Claude process, the Heylandt process and the Kapitza process reach the highest exergetic efficiencies (76.6%, 76.7% and 76.6), and have the lowest specific power requirement (1059, 1021 and 1059 kJ/kg$_{liquid\ air}$) and the highest liquid yields (0.609, 0.629, 0.609).

For the most efficient liquefaction configurations, the Claude-based processes, a sensitivity analysis was conducted. The compression pressure was varied (80–200 bar) and the splitting ratio r was reduced to its absolute minimum value. The effect of these variations on the exergetic efficiency ε can be seen in Figure 6. The share of air liquefied increases with a reduction in the value of the splitting ratio ($r = \dot{m}_{EX}/\dot{m}_{CM}$), as a greater mass flow enters the MHE and throttling process. The temperature difference in the MHE decreases with a reduction in "cold feed" ($\dot{m}_{EX}$) and a simultaneous increase in "hot feed" ($\dot{m}_{CM} - \dot{m}_{EX}$). The minimum splitting ratio is therefore restricted by the minimum pinch temperature ($\Delta T_{MHE1,\ min} \rightarrow 1$ K).
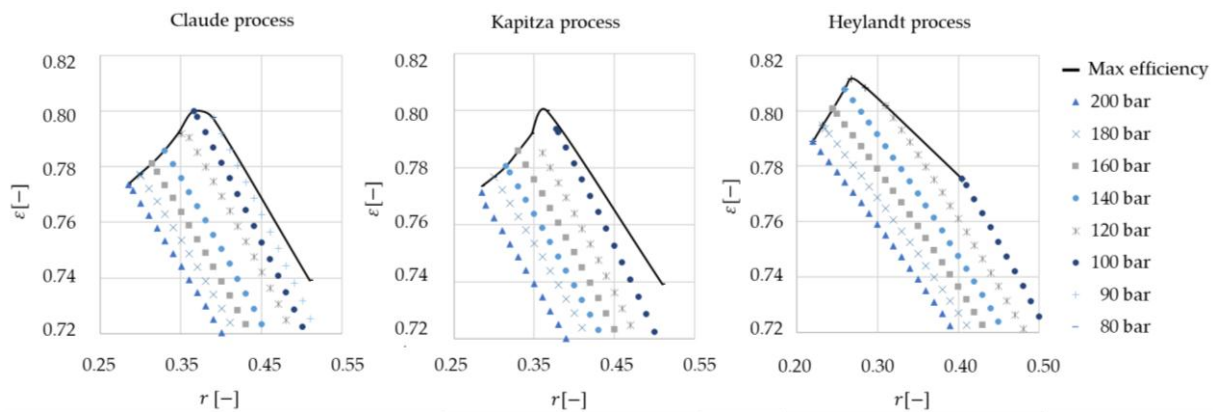
Figure 6. Sensitivity analysis results of the Claude, the Kapitza and the Heylandt process: exergetic efficiency ε over splitting ratio r, for various values of the liquefaction pressure. The maximum efficiency line is indicated with a solid black line.

By minimizing the splitting ratio for the respective compression pressure, a maximum efficiency line can be obtained. In Figure 7, the maximum exergetic efficiency curve of the Claude process, the Kapitza process and the Heylandt process are compared. The maximum liquid yield and the minimum specific power consumption graphs are also compared in Figures 8 and 9 respectively.

The thermodynamic performances of the Claude and Kapitza processes are almost the same. Reason for this is the temperature difference of only 3.3 K of the two mixing streams. The three processes reach their maximum efficiency at different pressures (Figure 7). This confirms that comparing the systems at a single pressure level is not sufficient. For liquefaction pressures of 120 bar and above the Heylandt process performs better reaching its optimum of approximately 81.2% (at 130 bar). The optimal configuration of the Claude and the Kapitza process is at about 100 bar reaching 80% exergetic efficiency.
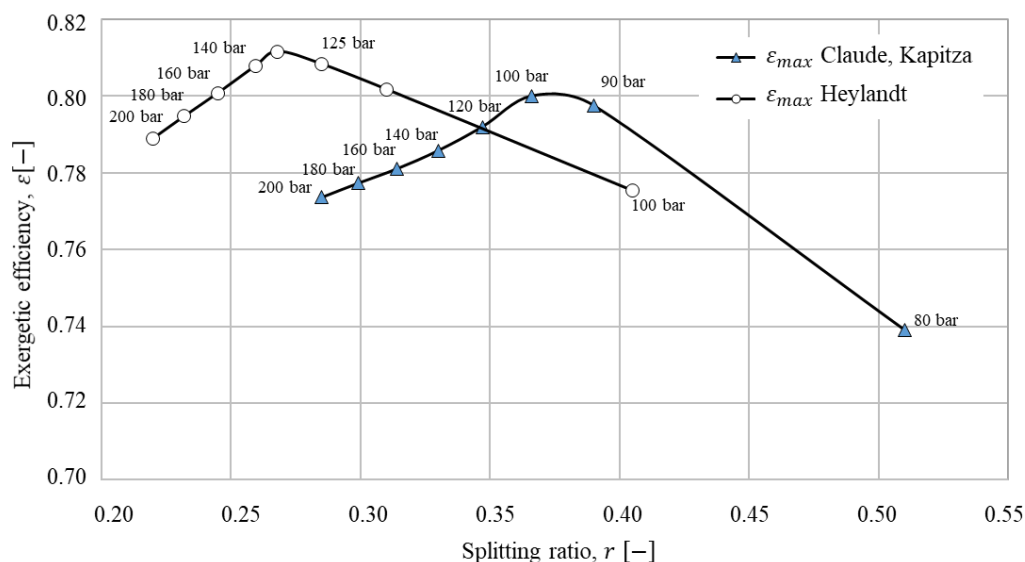

Figure 7. Maximum exergetic efficiency graphs as a function of the splitting ratio r for the Claude, Kapitza and Heylandt processes.
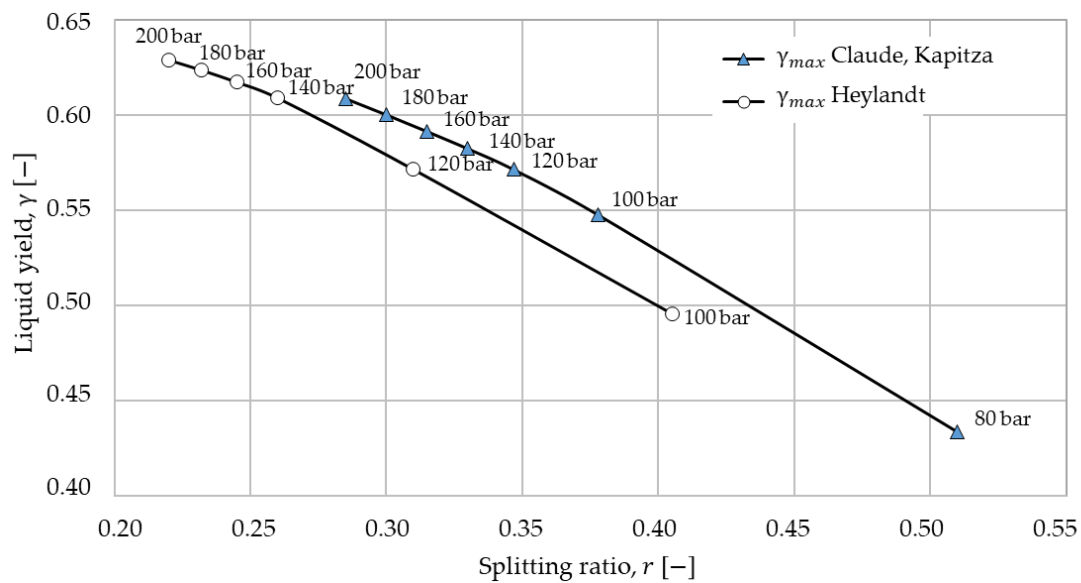
Figure 8. Maximum liquid yield graphs of the three Claude-based processes for different pressures and splitting ratios.
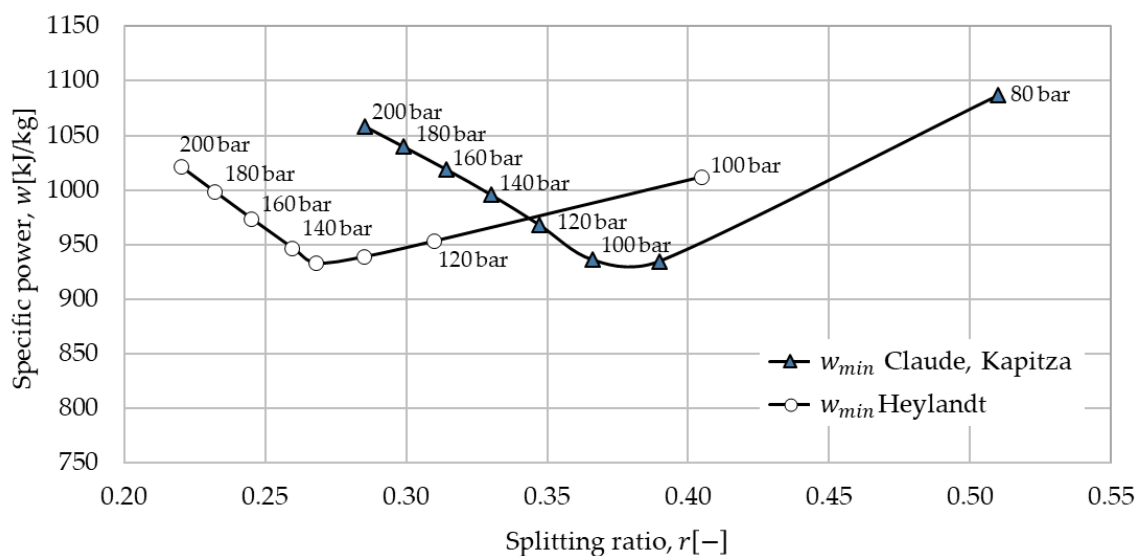

Figure 9. Minimum specific power graphs of the three Claude-based processes for different pressures and splitting ratios.

3.2. Economic Analysis

The economic analysis was conducted for the optimal system configuration for each of the three Claude-based systems. The system design parameters are given in Table 6. The charging power $\dot{W}_{char}$, the liquefaction capacity $\dot{m}_{liquid\ air}$, and the storage capacity $(\dot{W}_{dis} \cdot \tau_{dis})$ are similar for all systems. The liquid yield γ and the charging pressure p_{CM} of the Heylandt process is slightly higher.

Table 6. Design parameters for liquefaction systems evaluated in economic analysis.

Parameter	Unit	Claude	Heylandt	Kapitza
Liquefaction pressure	bar	95	130	95
Charging capacity	MW	20	20	20
Liquefaction capacity	tons/day	606	608	606
Storage capacity	MWh	76.6	78.4	76.6
Liquid yield	-	0.54	0.59	0.54

Figure 10 shows the BMC broken down to the component groups: expander, compressors, intercoolers, main heat exchanger and other components. The heat exchangers are responsible for 70–80% of the investment costs for all processes. The results of economic analysis of the Claude and the Kapitza process differ despite similar performance in energetic and exergetic analysis. The small difference in size of the MHE results in a noteworthy difference in costs. The total revenue requirements for the Claude, Heylandt and Kapitza systems amount to 2770 €/a, 2915 €/a and 2670 €/a respectively.
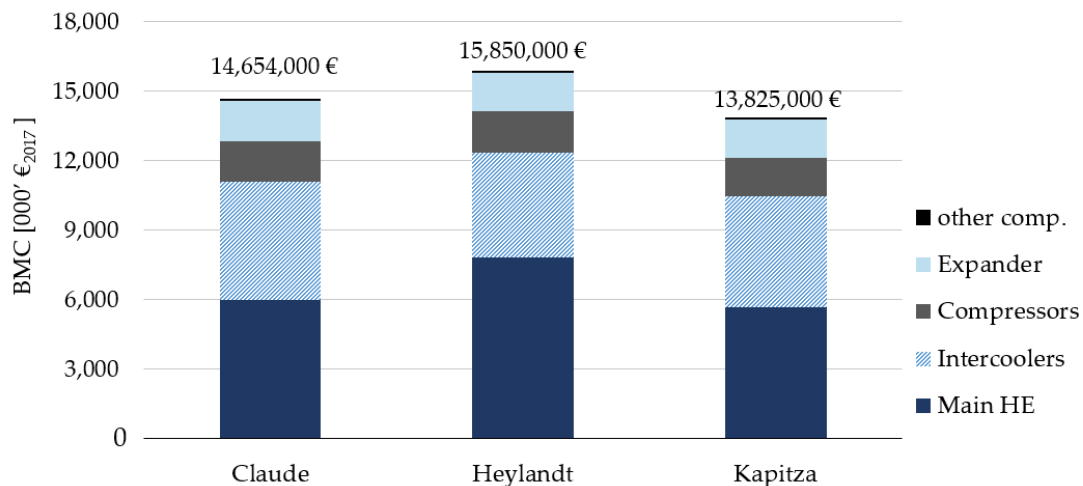

Figure 10. Bare module costs of the evaluated Claude-based systems with indicated cost shares of the contributing component groups.

The Heylandt system is not competitive in regards to its specific investment per unit of exergy stored despite the slightly higher energy output of the process, see Table 6. The specific investment per kW installed capacity for the Claude, Heylandt and Kapitza systems amount to 733 €/kW$_{char}$, 792 €/kW$_{char}$ and 691 €/kW$_{char}$, respectively.

3.3. Exergoeconomic Analysis

The results of the exergoeconomic analysis at the component level are shown in Figure 11. All analyzed systems show an elevated exergoeconomic factor ($f \gg 0.5$) which indicates that the costs associated with the purchase and maintenance of the components $\dot{Z}_k$ dominates the cost picture ($\dot{Z}_k \gg \dot{C}_{D,k}$). The cost of exergy destruction in the components $\dot{C}_{D,k}$ is a minor contributor to the costs of the final product. When investment costs dominate, a reduction in investment costs while accepting lower efficiencies is recommended to lower the total costs.

The exergoeconomic factor of several components in the Heylandt system is higher than in the other two systems. This indicates that the Heylandt system leaves more room for improvement of the cost-effectiveness of the system. Yet, regarding the significantly higher average cost per unit of exergy of the product $c_{P,tot}$ (Table 7), the reduction in costs may not be substantial enough to surpass the other configurations.

The average cost of exergy of the fuel $c_{F,tot}$ is relatively high in comparison to the low average cost of the electricity $c_{electricity} = 17.5$ €/MWh. Reason for this is the average cost of low-temperature exergy supplied by the cold storage $c_{q,cold}$ which is relatively high and amounts to the average cost of exergy of the liquid air $c_{liquid\ air}$. The average cost of exergy of the heat supplied to heat storage has the lowest value for the Heylandt process while the average cost of exergy of liquid air is the most expensive. Regarding the average cost of the exergy of the final product $c_{P,tot}$, the Kapitza process performs best.

This conclusion is not expected to be changed with increase in the system size. The reason is that the heat exchangers are the major contributors to the costs of the liquefaction systems, and the cost of heat exchanger increase linearly with scale—for all systems equally.
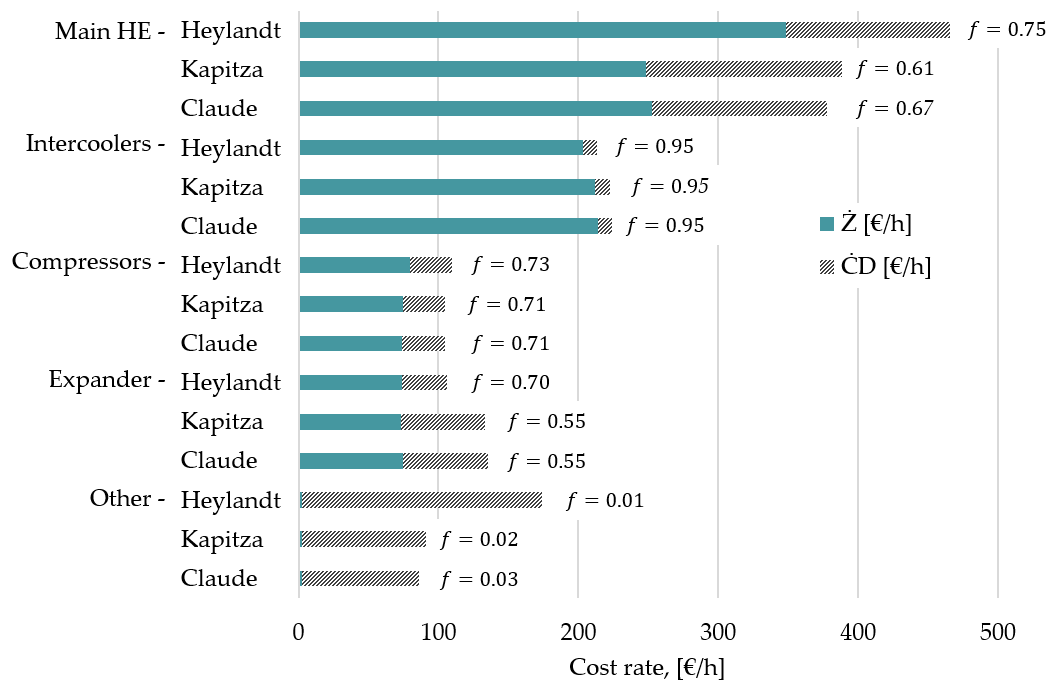
Figure 11. Sum of the cost rates associated with the initial investment of the component $\dot{Z}_k$ and the exergy destruction $\dot{C}_{D,k}$ and exergoeconomic factor f of the respective component(s).

Table 7. Results of exergoeconomic analysis for the three evaluated systems.

Parameter	Claude	Heylandt	Kapitza	Unit
Average cost of exergy of the fuel, $c_{F,tot}$	44.3	61.2	44.0	€/MWh
Average cost of exergy of the losses, $c_{L,tot}$	39.3	43.7	39.2	€/MWh
Average cost of exergy of the product, $c_{P,tot}$	88.8	114.8	88.0	€/MWh
Average cost of exergy of the liquid air, $c_{liquid\ air}$	95.4	133.4	94.6	€/MWh
Average cost of exergy of the heat, $c_{q,hot}$	67.9	63.1	67.5	€/MWh

No previous publications considered the effect of integrating cold storage on the selection of the liquefaction process. Thus, the results are validated by drawing comparison to values given in literature for air liquefaction processes without cold storage (Table 8) and values reported in previous publications for CES system characteristics (Table 9).

Table 8. Final results of the three Claude-based systems compared to air liquefaction processes.

Parameter	Unit	Claude	Heylandt	Kapitza	Reference
Specific power consumption	kWh/ton	264.0	263.3	264.0	520–760 [13], 439 [35]
Production cost of liquid air	€/ton	18.6	25.9	18.4	37–48 [35]

Table 9. Final results of the evaluation of the three Claude-based systems compared to CES system.

Parameter	Unit	Claude	Heylandt	Kapitza	Reference
CES specific investment	€/kW$_{dis}$	939	923	911	500–3000 [6,7,36]
CES round-trip efficiency	%	46.9	49.0	46.9	40–60 [6,9,36]

The specific power consumption of air liquefaction processes reported in [13] and [35] is twice as large than in the presented systems. The integration of cold storage thus not only decreases the specific power consumption to half but also reduces the production cost of liquid air from 37–48 €/ton [35] to 18.4–25.9 €/ton (Table 8).

Assuming a TCI for the 40 MW discharge unit of 17.1 Mio €, the specific investment of the CES systems based on the Claude processes reach values lower than 1000 €/kW$_{dis}$, see Table 9. The specific investment costs of the total CES system is approximated from 500–3,000 €/kW [6,7,36] in literature. The levelized cost of discharged electricity (LCOE$_{dis}$) of the CES systems based on the Claude, the Heylandt, and the Kapitza process are expected to reach 175.6 €/MWh$_{el}$, 175.3 €/MWh$_{el}$ and 172.0 €/MWh$_{el}$, respectively. For industrial application 120-200 €/MWh are set as goal. A sensitivity analysis of the LCOE and comparison to other technologies was reported in [34]. The final RTE of 47–49% are also in line with the expected 40–60%, which confirms the presented results.

In Table 10, the specific investment costs and RTE of other bulk-energy storage technologies are given. The competing bulk-energy storage technology are also capital intense which makes CES competitive with compressed air energy storage (CAES), pumped hydro storage (PHS) and hydrogen-based energy storage (H$_2$). Regarding the RTE of PHS and CAES, CES efficiency is still the greatest obstacle. The high exergy density of CES (120–200 kWh/m^3 [36])—the absence of geographical constraints—remains the technologies greatest advantage.

Table 10. Specific investment cost and RTE of competing bulk-energy technologies.

Parameter	Unit	CAES	PHS	H2
Specific investment cost	€/kWdis	500–2200 [37]	350–1,500 [37]	> 2000+ [38]
Round-trip efficiency	%	40–5 [37]	75–85 [39,40]	30–50 [38,41]
Exergy density	kWh/m^3	0.5–1.5 [36]	3–6 [36]	133–785 [41], 500+ [36]

4. Conclusions

This paper presents the state-of-the-art of cryogenic energy storage with regards to air liquefaction processes, thermodynamic parameters and cold storage configurations. Six air liquefaction processes within the charge unit of CES were investigated and results obtained from the exergy-based analysis were compared. The effect of cold storage integration on different liquefaction processes was firstly quantified.

- The integration of the charging unit with cold exergy recovery was shown to substantially augment the liquid yield γ, significantly reduce the specific power requirement w_{char} and significantly improve the exergetic efficiency ε of all liquefaction processes assessed.
- The simple Claude, the Heylandt and the Kapitza processes were found to reach the highest exergetic efficiencies and liquid yields, as well as the lowest specific power requirements for liquefaction.
- The sensitivity analysis showed that for liquefaction pressures of 125 bar and higher, the Heylandt process reaches the highest exergetic efficiencies, at lower pressures the Claude and the Kapitza process are superior.
- The economic analysis revealed that the Kapitza process-based system has the lowest specific investment cost and total revenue requirement.
- The exergoeconomic analysis demonstrated that the Kapitza process is the most cost-effective liquefaction process to be considered for CES with cold storage. The average cost of the exergy of the final product was the lowest in the Kapitza process.
- The results were compared to values from literature. The specific power consumption of the presented air liquefaction processes with cold storage ($\leq$264 kWh/ton) was found to be approximately half the values reported in literature. The production cost of liquid air was found to be significantly reduced with the integrating cold storage (18–26 €/ton).
- The final results on system level were found to be in line with the values reported for CES specific investment cost and RTE. Finally, CES was evaluated cost-competitive with other bulk-energy storage technologies.

Conflicts of Interest: The authors declare no conflict of interest.

References

1. Hamdy, S.; Morosuk, T.; Tsatsaronis, G. Cryogenic Energy Storage: Characteristics, Potential Applications and Economic Benefit. In *Recent Developments in Cryogenics Research*; Putselyk, S., Ed.; Nova Science, Inc.: New York, NY, USA, 2019; pp. 277–310.
2. Li, Y.; Chen, H.; Ding, Y. Fundamentals and applications of cryogen as a thermal energy carrier: A critical assessment. *Int. J. Therm. Sci.* **2010**, *49*, 941–949. [CrossRef]
3. Smith, E. Storage of Electrical Energy using Supercritical Liquid Air. *Proc. Inst. Mech. Eng.* **1977**, *191*, 289–298. [CrossRef]
4. European Energy Research Alliance. *Liquid Air Energy Storage, EERA Joint Program SP4—Mechanical Storage Fact Sheet 3*; European Energy Research Alliance: Brussels, Belgium, 2016.
5. Kishimoto, K.; Hasegawa, K.; Asano, T. *Development of Generator of Liquid Air Storage Energy System*; Mitsubishi Heavy Industries, Ltd.: Tokyo, Japan, 1998.
6. Morgan, R.; Nelmes, S.; Gibson, E.; Brett, G. An analysis of a large-scale liquid air energy storage system. In Proceedings of the Institution of Civil Engineers, London, UK, 1 September 2015.
7. Highview Enterprises Ltd. Highview Power Storage. 10 May 2018. Available online: http://www.highview-power.com/ (accessed on 15 December 2018).
8. Li, Y. Cryogen Based Energy Storage: Process Modelling and Optimization. Ph.D. Thesis, University of Leeds, Leeds, UK, 2011.
9. Hamdy, S.; Morosuk, T.; Tsatsaronis, G. Cryogenics-based energy storage: Evaluation of cold exergy recovery cycles. *Energy* **2017**, *138*, 1069–1080. [CrossRef]
10. Kerry, F.G. *Industrial Gas Handbook: Gas Separation and Purification*; Taylor & Francis Group, LLC: Boca Raton, FL, USA, 2007.
11. Ameel, B.; T'Joen, C.; De Kerpel, K.; De Jaeger, P.; Huisseune, H.; Van Belleghem, M. Thermodynamic analysis of energy storage with a liquid air Rankine cycle. *Appl. Therm. Eng.* **2013**, *52*, 130–140. [CrossRef]
12. Peng, H.; Shan, X.; Yang, Y.; Ling, X. A study on performance of a liquid air energy storage system with packed bed units. *Appl. Energy* **2018**, *211*, 126–135. [CrossRef]
13. Borri, E.; Tafone, A.; Romagnoli, A.; Comodi, G. A preliminary study on the optimal configuration and operating range of a "microgrid scale" air liquefaction plant for Liquid Air Energy Storage. *Energy Convers. Manag.* **2017**, *143*, 275–285. [CrossRef]
14. Abdo, R.F.; Pedro, H.T.; Koury, R.N.; Machado, L.; Coimbra, C.F.; Porto, M.P. Performance Evaluation of various cryogenic energy storage systems. *Energy* **2015**, *90*, 1024–1032. [CrossRef]
15. She, X.; Peng, X.; Nie, B.; Leng, G.; Zhang, X.; Weng, L.; Tong, L.; Zheng, L.; Wang, L.; Ding, Y. Enhancement of round trip efficiency of liquid air energy storage through effective utilization of heat of compression. *Appl. Energy* **2017**, *206*, 1632–1642. [CrossRef]
16. Sciacovelli, A.; Vecchi, A.; Ding, Y. Liquid air energy storage (LAES) with packed bed cold thermal storage—From component to system level performance through dynamic modelling. *Appl. Energy* **2017**, *190*, 84–98. [CrossRef]
17. Morgan, R.; Nelmes, S.; Gibson, E.; Brett, G. Liquid air energy storage—Analysis and first results from pilot scale demonstration plant. *Appl. Energy* **2015**, *137*, 845–853. [CrossRef]
18. Guizzi, G.L.; Manno, M.; Tolomei, L.M.; Vitali, R.M. Thermodynamic analysis of a liquid air energy storage system. *Energy* **2015**, *93*, 1639–1647. [CrossRef]
19. Xue, X.; Wang, S.X.; Zhang, X.L.; Cui, C.; Chen, L.; Zhou, Y.; Wang, J. Thermodynamic analysis of a novel liquid air energy storage system. *Phys. Procedia* **2015**, *67*, 733–738. [CrossRef]

20. Peng, X.; She, X.; Cong, L.; Zhang, T.; Li, C.; Li, Y.; Wang, L.; Tong, L.; Ding, Y. Thermodynamic study on the effect of cold and heat recovery on performance of liquid air energy storage. *Appl. Energy* **2018**, *221*, 86–99. [CrossRef]

21. Chen, H.; Ding, Y.; Peters, T.; Berger, F. A method of storing energy and a cryogenic energy storage system. US Patent EP1989400A1, 27 February 2006.

22. Li, Y.; Cao, H.; Wang, S.; Jin, Y.; Li, D.; Wang, X.; Ding, Y. Load shifting of nuclear power plants using cryogenic energy storage technology. *Appl. Energy* **2014**, *113*, 1710–1716. [CrossRef]

23. Barron, R.F. *Cryogenic Systems*, 2nd ed.; Oxford University Press, Clarendon Press: New York, NY, USA; Oxford, UK, 1985.

24. Herron, D.M.; Agrawal, R. *Air Liquefaction: Distillation*; Air Products and Chemicals, Inc.: Allentown, PA, USA, 2000.

25. Brett, G.; Barnett, M. The application of liquid air energy storage for large scale long duration solutions to grid balancing. *EPJ Web Conf.* **2014**, *79*, 03002. [CrossRef]

26. Highview Power Storage Ltd. *Performance and Technology Review*. March 2012. Available online: https://businessdocbox.com/Green_Solutions/77092496-Highview-power-storage-technology-and-performance-review.html (accessed on 1 January 2019).

27. Bejan, A.; Tsatsaronis, G.; Moran, M. *Thermal Design and Optimization*; John Wiley & Sons Inc.: New York, NY, USA, 1996.

28. Morosuk, T.; Tsatsaronis, G. Splitting physical exergy: Theory and application. *Energy* **2019**, *167*, 698–707. [CrossRef]

29. Ulrich, G.D.; Vasudevan, P.T. Chapter 5 Capital Cost Estimation. In *Chemical Engineering—Process Design and Economics—A Practical Guide*; Process Publishing: New Hampshire, NH, USA, 2004; pp. 352–419.

30. Peters, M.S.; Timmerhaus, K.D.; West, R.E. Chapter 12 Materials-Handling Equipment—Design and Costs. In *Plant Design and Economics of Chemical Engineers*; McGraw-Hill Companies, Inc.: New York, NY, USA, 2003; pp. 485–589.

31. Xu, G.; Liang, F.; Yang, Y.; Hu, Y.; Zhang, K.; Liu, W. An Improved CO_2 Separation and Purification System Based on Cryogenic Separation and Distillation Theory. *Energies* **2014**, *7*, 3484–3502. [CrossRef]

32. Smith, R. *Chemical Process Design and Integration*; John Wiley & Sons, Ltd.: Manchester, UK, 2014.

33. Chemical Engineering. Available online: https://www.chemengonline.com/cepci-updates-january-2018-prelim-and-december-2017-final/ (accessed on 12 September 2018).

34. Hamdy, S.; Morosuk, T.; Tsatsaronis, G. Exergetic and economic assessment of integrated cryogenic energy storage systems. *Cryogenics* **2019**. accepted manuscript.

35. Strahan, D.; Akhurst, M.; Atkins, D.A.; Arbon, P.I.; Ayres, M. *Liquid Air in the Energy and Transport Systems*; Center for Low Carbon Futures: York, UK, 2013.

36. Chen, H.; Cong, T.N.; Yang, W.; Tan, C.; Li, Y.; Ding, Y. Progress in electrical energy storage system: A critical review. *Prog. Nat. Sci.* **2009**, *19*, 291–312. [CrossRef]

37. EERA/EASE. European Association for Storage of Energy. Available online: http://ease-storage.eu/wp-content/uploads/2015/10/EASE-EERA-recommendations-Roadmap-LR.pdf (accessed on 16 January 2019).

38. Welder, L.; Stenzel, P.; Ebersbach, N.; Markewitz, P.; Robinius, M.; Emonts, B.; Stolten, D. Design and Evaluation of Hydrogen Electricity Reconversion Pathways in National Energy Systems Using Spatially and Temporally Resolved Energy System Optimization. *Int. J. Hydrog. Energy* **2018**, in press. [CrossRef]

39. Ibrahim, H.; Ilinca, A.; Perron, J. Energy storage systems—Characteristics and comparisons. *Renew. Sustain. Energy Rev.* **2008**, *12*, 1221–1250. [CrossRef]

40. Kaldellis, J.K.; Zafirakis, D. Optimum energy storage techniques for the improvement of renewable energy sources-based electricity generation economic efficiency. *Energy* **2007**, *32*, 2295–2305. [CrossRef]

41. Li, Y.; Chen, H.; Zhang, X.; Tan, C.; Ding, Y. Renewable energy carriers: Hydrogen or liquid air/nitrogen? *Int. J. Therm. Sci.* **2010**, *49*, 941–949. [CrossRef]